



**HAL**  
open science

# Finite element modeling of indentation and adhesive wear in sliding of carbon fiber reinforced thermoplastic polymer against metallic counterpart

Israr Ud Din, Stéphane Panier, Pei Hao, Gérald Franz, Jayashree Bijwe, Li Hui

## ► To cite this version:

Israr Ud Din, Stéphane Panier, Pei Hao, Gérald Franz, Jayashree Bijwe, et al.. Finite element modeling of indentation and adhesive wear in sliding of carbon fiber reinforced thermoplastic polymer against metallic counterpart. *Tribology International*, 2019, 135, pp.200 - 212. 10.1016/j.triboint.2019.03.010 . hal-03485094

**HAL Id: hal-03485094**

**<https://hal.science/hal-03485094>**

Submitted on 20 Dec 2021

**HAL** is a multi-disciplinary open access archive for the deposit and dissemination of scientific research documents, whether they are published or not. The documents may come from teaching and research institutions in France or abroad, or from public or private research centers.

L'archive ouverte pluridisciplinaire **HAL**, est destinée au dépôt et à la diffusion de documents scientifiques de niveau recherche, publiés ou non, émanant des établissements d'enseignement et de recherche français ou étrangers, des laboratoires publics ou privés.



Distributed under a Creative Commons Attribution - NonCommercial 4.0 International License

## Finite element modeling of indentation and adhesive wear in sliding of carbon fiber reinforced thermoplastic polymer against metallic counterpart

Israr Ud Din<sup>1,4\*</sup>, Stéphane Panier<sup>1</sup>, Pei Hao<sup>1</sup>, Gérald Franz<sup>1</sup>, Jayashree Bijwe<sup>2</sup>, Li Hui<sup>3</sup>

1. Laboratoire des Technologies Innovantes, LTI-EA 3899, Université de Picardie Jules Verne, Amiens, 80025, France
2. Industrial Tribology Machine Dynamics and Maintenance Engineering Center (ITMMEC), Indian Institute of Technology Delhi, Hauz Khas, New Delhi, 110016, India
3. School of Mechatronics Engineering, Shenyang Aerospace University, Shenyang, China
4. Research Center for Modeling & Simulation (RCMS), National University of Sciences and Technology (NUST), Islamabad, Pakistan

### \*Corresponding Author:

**Israr Ud Din, PhD**

Laboratoire des Technologies Innovantes (LTI), LTI-EA 3899,

Université de Picardie Jules Verne, Amiens, France.

Email address: (israr.uddin@u-picardie.fr), (israr.rcms@rcms.nust.edu.pk)

---

\*Corresponding author.

Email addresses: israr.uddin@u-picardie.fr , israr.rcms@rcms.nust.edu.pk (Israr Ud Din)

Finite element modeling of indentation and adhesive wear in sliding of carbon fiber reinforced thermoplastic polymer against metallic counterpart

## ABSTRACT

In this work, adhesive wear in uni-directional (UD) reinforced carbon thermoplastic Polyetherimide (PEI) composite laminate caused by the sliding of a metallic counterpart is analyzed. The study is based on the finite element method (FEM) in various in-plane directions of sliding relative to fibers. The damage and failure mechanisms induced by the adhesive wear are predicted with 3D Hashin's theory and Puck's theory. These failure theories were implemented in ABAQUS via UMAT in implicit environment. The damage mechanisms predicted by the FEM model showed a better correspondence with the observed damage modes in the wear experiments of fiber reinforced polymers (FRPs). Furthermore, specific failure exposure factors were also compared with the specific wear rates determined experimentally in a qualitative manner.

Keywords: Adhesive wear, 3D Puck's theory, Finite element modeling, Wear damage mechanisms.

## 1. Introduction

Fiber reinforced polymers (FRPs), specifically thermoplastics (PEEK, PES, PEI, etc.) reinforced by carbon fibers (CFs), are used in the elevated temperature applications in tribo-components where harsh operating conditions prevail such as in aircrafts. Previous studies show that CFs in the tribo-systems offer partial lubricity in addition to higher specific strength, thermal conductivity, resistance to fatigue and damage, etc. [1, 2]. Such material combinations provide other advantages including recyclability in contrary to thermoset polymers as epoxy and unlimited shelf life [1]. It is important to study numerically the damage induced by the contact of two counterparts and the subsequent wear in FRPs. However, this numerical analysis of wear process is a very complex task to accomplish. Different types of fibers, their properties and fiber volume ratio make the numerical analysis of this process further difficult. Wieleba [3] described that the dominant wear process during the rubbing of fibrous composites is the adhesion. But depending on the type of fibers and friction conditions, other wear mechanisms may also be encountered. Fundamental factors that influence the wear of fibrous composite materials include

fiber type, fiber volume ratio in the composite, and the properties of the fiber/matrix interface. This study focuses on the UD based FRPs composite laminates under in-plane wear conditions.

Wear phenomenon in FRPs has been studied experimentally and literature is available for different modes of wear including abrasive wear and adhesive wear [1, 4, 5]. Cirino et al. [5] investigated the dry abrasive-dominant wear in UD composite in which the composite was worn in three principal directions. These three directions were designated as N (Normal), P (Parallel) and AP (Anti-Parallel) with respect to the fiber orientation as shown in Fig.1. P and AP wear directions are in-plane while wear in N-direction is out-of-plane and is not considered in this study.

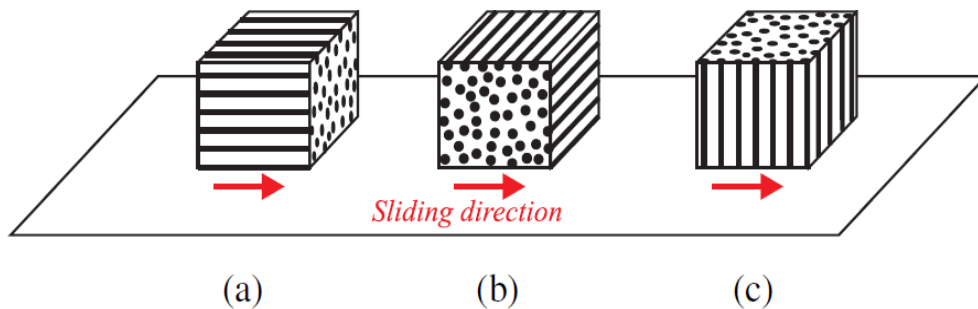


**Fig. 1:** Three principal sliding directions with respect to fiber, (a) Parallel (P), (b) Anti-Parallel (AP), (c) Normal (N) [6]

The damage mechanisms encountered in the abrasive and adhesive types of wear were studied using scanning electron microscopy (SEM) in each direction of sliding in the experiments [1, 2, 7, 8]. In case of wear in direction P, a typical SEM micrograph can be seen in Fig. 2 [7]. This figure shows different failure mechanisms during the wear process in FRPs composite. These comprise fiber/matrix de-bonding, fiber bending, fiber cracking and matrix shear features. It is noticeable in Fig. 2-a that the polished surface remained in its undamaged state away from the groove scratched by the diamond tip indenter. At higher magnification (see Fig. 2-b), a fiber crack transferring from one fiber to the next is noticeable. In addition, the formation of shear features can also be seen.

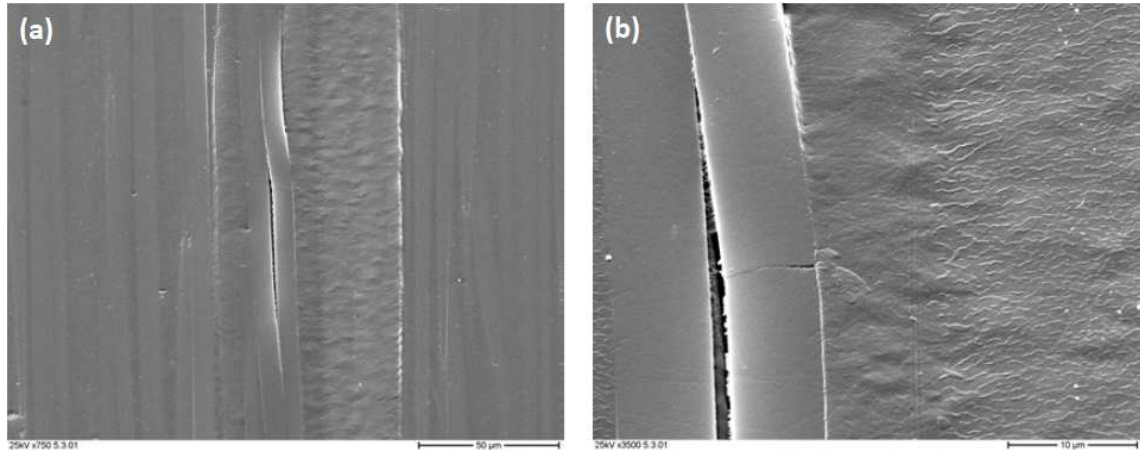


**Fig. 2:** (a) SEM micrograph of P-direction composite surface scratched by a diamond tip indenter, (b) an enlarged view [7]

Similarly, Fig. 3 depicts the damage mechanisms when a FRPs composite is scratched by a diamond tip indenter in AP-direction. Due to the compressive and frictional loads, fiber bending takes place in the depth direction (out-of-plane bending) and also in the sliding direction (in-plane bending). Both in-plane and out-of-plane bending ultimately contribute to fiber fracture in the central region of the groove as well as in the transition between the groove and the undamaged area. The damage mechanisms are similar to the P-direction scratch including fiber/matrix de-bonding, shear features of the matrix material between the broken fibers, fiber cracking and their removal from the fiber beds. Friedrich et al. [9] emphasized that if the diamond tip indenter is replaced with a small steel ball, the characteristic wear and damage mechanisms are very similar but these are not seen clearly as in case of the damage mechanisms produced by the diamond indenter.

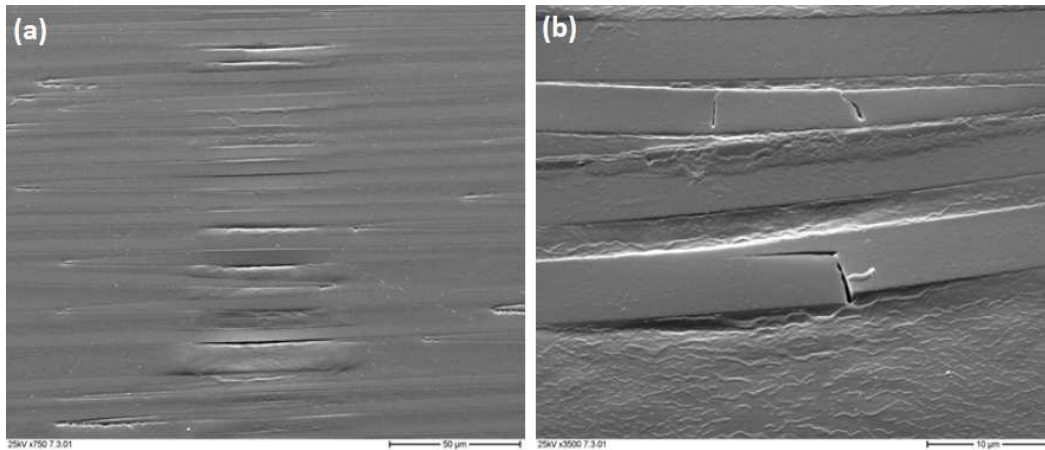


**Fig. 3:** (a) SEM micrograph of AP-direction composite surface scratched by a diamond tip, (b) a magnified view of the groove [7]

Friedrich et al. [7] explained that wear process takes place in a sequence of damage mechanisms and these were termed as wear cycles. Accordingly, the wear cycle initiates from the matrix wear and fiber sliding wear. Fiber sliding wear is also known as fiber thinning in the literature. These are followed by fiber cracking and fiber/matrix de-bonding at the interface. When the wear process reaches the steady state then a so-called compacted wear debris layer (CWDL) covers the surface which is composed of pulverized fibers and matrix material. During the wear process, this layer is continuously formed and removed by the surfaces sliding against each other. The preceding studies were limited to only three directions comprising P, AP and N. Sharma et al. [2, 8] carried out experimental studies in various fiber directions. UD carbon reinforced thermoplastics (PEI) with 80% by volume were tested at range of angles as  $0^\circ$ ,  $30^\circ$ ,  $45^\circ$ ,  $60^\circ$  and  $90^\circ$  during abrasive wear [8] and in dry-adhesive wear [2]. The increase in the coefficient of friction ( $\mu$ ) was reported as the fiber angle with respect to the sliding direction was increased. In addition, very low specific wear rate (*volume removed per unit of work required =  $K_0$ , unit:  $mm^3 / N.m$* ) was determined for the sliding in the fiber direction (P-direction). On the other hand, the specific wear rate in AP-direction ( $90^\circ$ ) in the experiments was computed as four times higher than the P-direction ( $0^\circ$ ). Ovaert [10] reported similar results by conducting wear experiments on fiber reinforced thermoset epoxy matrix. Sharma et al. concluded that sliding orthogonal to the fiber (AP-direction) leads to higher wear. In addition, they highlighted that in AP-direction, FRPs are more vulnerable to de-bonding, peel-off the plies and the pulverization of fibers as compared to the P-direction sliding.

In contrast to the experimental work on the wear of FRPs, very few studies have reported on modeling the damage mechanisms encountered in the wear process. Most of the wear modeling and the corresponding damage mechanisms are based on the micro-mechanics approach considering multi-phase materials in a single ply: stiffer fiber, softer matrix and weaker fiber/matrix interface [9, 11]. A sliding hemispherical asperity was modeled to correlate the damage modes observed in the experiment of PEEK with the finite element method (FEM) based results [9]. Slah et al. [11] modeled glass fiber and epoxy with Johnson-Cook (JC) behavior law [12], and fiber/matrix de-cohesion was assumed to follow the cohesive zone approach in ABAQUS/Explicit. Slah et al. [11] highlighted that experimental approaches are insufficient for better comprehension of the wear behavior of composite materials. Hence, these shall be supplemented with the FEM simulations. In contrast to the previous multi-phase material numerical modeling discussed above, a single ply is considered as orthotropic homogenized continuum in the present work. This approach is known as meso-scale and has been adopted in numerous studies [13-15] for the prediction of fiber fracture and matrix fracture in quasi-static loading. In these models, the elastic and strength values of a single homogenized ply are provided as inputs instead of the constituents: fiber, matrix and interface. The application of a better failure theory for the damage prediction in wear keeping in view the accuracy and which distinguishes between the fiber fracture and inter fiber fracture (matrix fracture and de-bonding) are the important characteristics of the study presented here. The application of homogenized ply approach or the meso-scale approach in modeling the damage mechanisms in wear is not available in the literature. This approach reduces the complexity in modeling. In addition, the computation cost is considerably reduced but similar damage mechanisms can be interpreted as in case of micro-mechanics based modeling of wear. 3D Puck's theory [16] is used to predict the damage due to wear and frictional contact problem in a UD laminate in order to better understand the insights. It is best suited due to its accuracy and stress interaction capability particularly when the transverse normal stress becomes compressive. When transverse compressive stress is increased, friction between the sliding material surfaces increases as a function of the normal compressive stress. Consequently, the material becomes capable to resist higher shear stress. The intra-laminar damage prediction capability of Puck's theory has been demonstrated in various scientific studies in referenced to the experiments [13, 14]. For comparison, 3D Hashin's failure theory [17] is also used. Finally, the FEM results based on both

the theories are compared with the experimental results of Sharma et al. [2]. In a single laminate, all the plies are considered in one direction. Therefore, there are fewer chances of delamination, and hence it is not considered in FEM modeling in the sequel.

## 2. Finite Element Modeling

### 2.1 Simulation set-up and boundary conditions (BCs)

In our study, finite element model is developed and the damage is detected by employing 3D Puck's theory [16, 18] and 3D Hashin's theory [17] in a homogenized orthotropic ply. The contact stresses and strains are analyzed to better understand the damage mechanisms in adhesion wear by sliding a hemispherical steel indenter on FRPs sample as illustrated in Fig. 4 [9].  $F_N$ ,  $F_T$  and  $F_R$  express the normal applied force, tangential force and the resultant force, respectively. In addition,  $2a$  and  $2b$  denote the minor and major axes of the elliptical contact area in the sliding direction and transverse direction. The radius of the metallic indenter is  $R=0.25$ mm. Failure theories which are used here are fully capable of detecting each type of damage mechanisms such as fiber fracture, matrix fracture, and fiber/matrix de-bonding based on the magnitudes of the contact stresses in the fiber and matrix materials. After the prediction of damage mechanisms using the failure theories, these will be correlated with wear damage mechanisms witnessed in the experiments of FRPs.

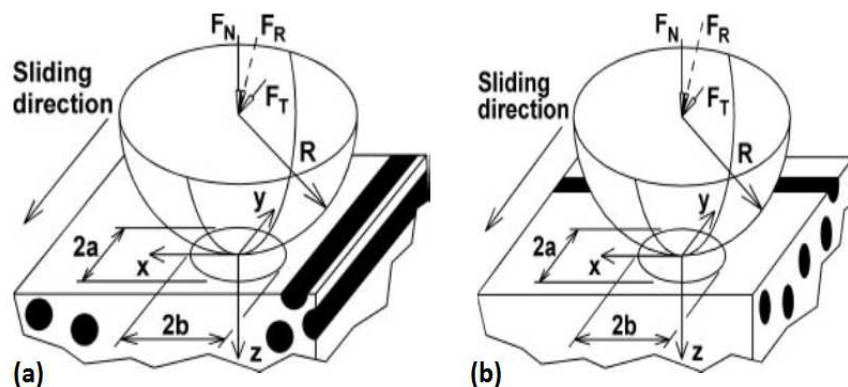


**Fig. 4:** Schematics of indentation and sliding (a) Parallel sliding to fibers (P), (b) Orthogonal sliding to fibers (AP) [9]

The composite material system used in the FEM analysis is based on the Polyetherimide (PEI) resin and UD reinforced CFs in 80% by volume. Sharma et al. [8] fabricated the composite

samples by compression molding after optimizing the important parameters. UD Laminates with different fiber orientations were characterized for various material properties such as tensile (ASTM D-638), in-plane shear strength (Iosipescu-ASTM D-5379/D- 5379M) and inter-laminar shear strength (ILSS) (ASTM 2344) [2]. The mechanical properties of the composite (CF-PEI) are listed in Table 1. The uniqueness of this material is its bad adhesion between the fiber and matrix which can be noticed by a lower value of the transverse tensile strength  $R_{\perp}^t$ . Similar notations are used here for consistency which were used by Puck et al. [16]. Accordingly, the symbol  $\parallel$  defines fiber direction ‘1’ and  $\perp$  denotes the in-plane transverse ‘2’ and out-of-plane direction ‘3’ in the materials principal axis.

**Table 1:** Engineering constants and mechanical strengths of CF-PEI [8]

$E_{\parallel}$ (MPa)	$E_{\perp}$ (MPa)	$G_{\perp\parallel}$ (MPa)	$G_{\perp\perp}$ (MPa)	$R_{\parallel}^t$ (MPa)	$R_{\parallel}^c$ (MPa)	$R_{\perp}^t$ (MPa)	$R_{\perp}^c$ (MPa)	$R_{\perp\parallel}$ (MPa)
130000	7600	6400	3000	518.0	500.0	7.0	105.0	40.0
			$\nu_{\perp\parallel}$	$\nu_{\perp\perp}$	$R_{\perp}$ (MPa)			
			0.21	0.25	18.0			

$E_{\parallel}, E_{\perp}, G_{\perp\parallel}, G_{\perp\perp}, \nu_{\perp\parallel}, \nu_{\perp\perp}$  denote the elastic constants in the material local axis.  $R_{\parallel}^t, R_{\parallel}^c, R_{\perp}^t, R_{\perp}^c, R_{\perp\parallel}$  are the strengths of the UD ply in the material principal axis where superscripts ‘t’ and ‘c’ describe the tension and compression. Fig. 5 elaborates the geometry, mesh constructions and the boundary conditions (BCs) adopted in the model. In order to reduce the CPU time, only the zone of interest in the specimen is modeled. Hence, the sample having dimensions of  $0.5 \times 0.5 \times 1 \text{ mm}^3$  was divided into three rectangular parallelepiped parts. The bottom face of the sample was constrained while x-symmetry condition was applied on the vertical mid-surface of the specimen parallel to Y-Z plane in the coordinate system shown in Fig. 5.

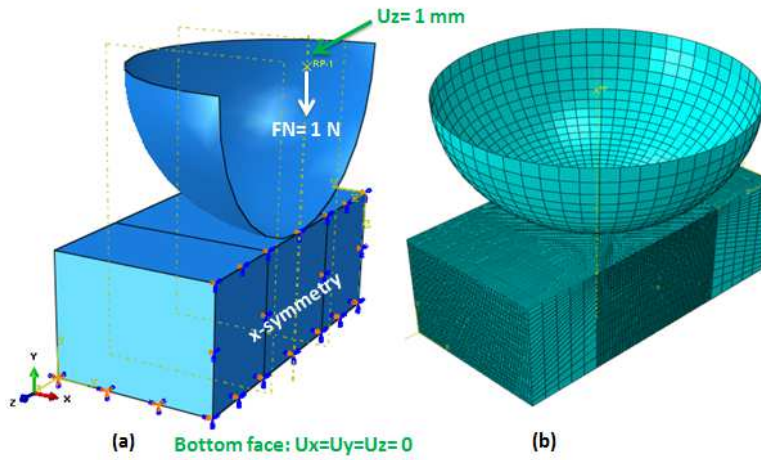


**Fig. 5:** Simulation set-up (a) BCs, (b) FEM mesh

A 3D 8-node continuum element C3D8 was employed for meshing the specimen having homogenized orthotropic properties of CF-PEI. In the FEM model, total 223135 finite elements were used based on the mesh convergence study. The mesh discretization was purposely refined close to the contact zone between the indenter and the composite where elements of edge size 0.005 mm were used. The interaction between the indenter and the sample was controlled by the contact pairs' algorithm in which surface to surface contact with slave surface type and node region was defined. In accordance with the experimental studies of Sharma et al. [2], all interactions followed the Coulomb friction model with an interfacial friction coefficient ( $\mu$ ) of about 0.28 (P-direction sliding) and 0.3 (AP-direction sliding). Furthermore, two steps were defined to simulate the sliding of the indenter in ABAQUS/Standard: (i) indentation step, (ii) sliding step. A vertical load  $F_N = 1\text{ N}$  was applied on the indenter up to the target penetration in the composite sample (see Fig. 5-a). In the sliding step, the scratching began with the indenter tangential sliding until the target scratch length of 0.05 mm was achieved. As seen in Fig. 5-a, displacement load in the z-direction was applied.

## 2.2 3D Puck's theory

For the intra-laminar damage due to wear, 3D Puck's theory [16, 18] is used and implemented via UMAT in ABAQUS. There are about twenty failure theories which are available as a conclusion from the World Wide Failure Exercises (WWFEs) [19-22]. WWFEs and other studies have shown the accuracy of Puck's criterion to predict the failure of FRPs. Recent articles reveal that this criterion can also be used as a good indicator to detect the meso-damage initiation in

continuum damage mechanics (CDM) models [13, 15]. Furthermore, crack orientation and the degree of severity of the fracture can also be distinguished due to the physical background of Puck's theory. Yet, it still uses the same number of strength parameters required for other conventional failure theories. The 3D form of Puck's theory is given in Eqn. (1). In Puck's theory, inter fiber fracture (IFF) signifies the matrix fracture in a lamina which is formed by the coalescence of diffused damages (matrix micro-cracking and fiber/matrix de-bonding). The stress exposure factor for tension in fiber direction is denoted by  $f_{E,FF,+}$  and the corresponding exposure factor for compression as  $f_{E,FF,-}$ . Likewise, the stress exposure factor in transverse tension in matrix dominant direction is expressed by  $f_{E,IFF,+}$  and the corresponding exposure factor in transverse compression as  $f_{E,IFF,-}$ . Readers are referred to [16, 18, 23] for further details of Puck's theory. These damage exposure factors will be evaluated in indentation and sliding.

$$\begin{aligned}
f_{E,FF,+} &= \frac{1}{R_{\parallel}^t} \left[ \sigma_{11} - \left( v_{\perp\parallel} - \frac{E_{\parallel}}{E_{\parallel f}} v_{\perp\parallel f} \right) (\sigma_{22} + \sigma_{33}) \right] = 1 ; & \sigma_{11} \geq 0 \\
f_{E,FF,-} &= \frac{1}{R_{\parallel}^c} \left[ \sigma_{11} - \left( v_{\perp\parallel} - \frac{E_{\parallel}}{E_{\parallel f}} v_{\perp\parallel f} m_{\sigma f} \right) (\sigma_{22} + \sigma_{33}) \right] = 1 ; & \sigma_{11} < 0 \\
f_{E,IFF,+} &= \sqrt{\left[ \left( \frac{1}{R_{\perp}^A} - \frac{p_{\perp\psi}^t}{R_{\perp\psi}^A} \right) \sigma_n(\theta) \right]^2 + \left( \frac{\tau_{nt}(\theta)}{R_{\perp\perp}^A} \right)^2 + \left( \frac{\tau_{n1}(\theta)}{R_{\perp\parallel}^A} \right)^2} + \frac{p_{\perp\psi}^t}{R_{\perp\psi}^A} \sigma_n(\theta) = 1 ; & \sigma_n \geq 0 \\
f_{E,IFF,-} &= \sqrt{\left( \frac{p_{\perp\psi}^c}{R_{\perp\psi}^A} \sigma_n(\theta) \right)^2 + \left( \frac{\tau_{nt}(\theta)}{R_{\perp\perp}^A} \right)^2 + \left( \frac{\tau_{n1}(\theta)}{R_{\perp\parallel}^A} \right)^2} + \frac{p_{\perp\psi}^t}{R_{\perp\psi}^A} \sigma_n(\theta) = 1 ; & \sigma_n < 0
\end{aligned} \tag{1}$$

Where  $\psi$  is the angle between the shear stress components on the fracture plane and can be calculated as:

$$\cos^2 \psi = \frac{\tilde{\tau}_{nt}^2}{\tilde{\tau}_{nt}^2 + \tilde{\tau}_{n1}^2}; \quad \sin^2 \psi = \frac{\tilde{\tau}_{n1}^2}{\tilde{\tau}_{nt}^2 + \tilde{\tau}_{n1}^2} \tag{2}$$

The stress components on the fracture plane can be computed by the transformation of the stress tensor from the ply local Cartesian coordinate system to the fracture plane:

$$\begin{bmatrix} \sigma_n(\theta) \\ \tau_{nt}(\theta) \\ \tau_{ni}(\theta) \end{bmatrix} = \begin{bmatrix} \cos^2 \theta & \sin^2 \theta & 2\sin \theta \cos \theta & 0 & 0 \\ -\cos \theta \sin \theta & \cos \theta \sin \theta & \cos^2 \theta - \sin^2 \theta & 0 & 0 \\ 0 & 0 & 0 & \sin \theta & \cos \theta \end{bmatrix} \begin{bmatrix} \sigma_{22} \\ \sigma_{33} \\ \sigma_{23} \\ \sigma_{13} \\ \sigma_{12} \end{bmatrix} \quad (3)$$

In the above equation, all the stress components except the stress in the fiber direction  $\sigma_{11}$  contribute to the matrix intra-laminar fracture.  $\sigma_n(\theta)$  is the stress component which is normal to the fracture plane,  $\tau_{nt}(\theta)$  is the in-plane shear stress parallel to the fibers and,  $\tau_{ni}(\theta)$  is the through-thickness shear stress (t stands for the transverse direction shear stress). Due to the fact that the stresses on the fracture plane have three components, therefore, three strength parameters are required for the failure envelope to provoke the damage onset. These fracture strengths are denoted as:  $R_{\perp}^{At} = R_{\perp}^t$ ,  $R_{\perp\parallel}^A = R_{\perp\parallel}$  and  $R_{\perp\perp}^A = \frac{R_{\perp}^c}{2(1+p_{\perp\perp}^c)}$ . Alternately,  $R_{\perp\perp}^A$  can also be computed by knowing the angle of pure transverse compression experimentally as:  $R_{\perp\perp}^A = \frac{R_{\perp}^c}{2(1+\tan \theta)}$ . Here  $R_{\perp}^t$ ,  $R_{\perp\parallel}$  and  $R_{\perp}^c$  are the tensile strength in transverse direction, in-plane shear strength and transverse compressive strength. Superscripts ‘A’, ‘t’ and ‘c’ express the ‘action plane’, ‘tension’ and ‘compression’. When pure transverse tensile stress or pure in-plane shear stress is applied on a UD lamina then the fracture plane is coincident with the action plane. Hence the action plane strength is same as the conventional strength obtained by ASTM testing [23]. In contrast, a single compressive stress cannot separate the material in its action plane rather the fracture plane is oblique. The failure is the sliding mode, and hence it is attributed to the resultant of shear stresses on the fracture plane:  $\tau_{n\psi} = \sqrt{\tau_{ni}^2 + \tau_{nt}^2}$ . Therefore, the out-of-plane shear strength of the action plane  $R_{\perp\perp}^A$  is determined from the transverse compressive test. The Puck’s envelope inclination points are enlisted in Table 2 for CFRPs and GFRPs [18] obtained from extensive experiments.

**Table 2:** Inclination parameters [18]

Material	$p_{\perp\perp}^t$	$p_{\perp\perp}^c$	$p_{\parallel\perp}^t$	$p_{\parallel\perp}^c$	$m_{\sigma_f}$
GFRPs	0.30	0.25	0.20	0.25	1.3

<b>CFRPs</b>	0.35	0.30	0.25	0.30	1.1
--------------	------	------	------	------	-----

The generalized inclination parameters as a function of the angle  $\psi$  in Eqn. (1) are computed with the help of the following relations:

$$\frac{P_{\perp\psi}^i}{R_{\perp\psi}^A} = \frac{P_{\perp\perp}^i}{R_{\perp\perp}^A} \cos^2 \psi + \frac{P_{\perp\parallel}^i}{R_{\perp\parallel}^A} \sin^2 \psi; \quad i = t, c \quad (4)$$

The four stress exposure factors of the Puck's theory as given in Eqn. (1) will be evaluated for P-direction and AP-direction sliding configurations of steel indenter on the UD FRPs specimen. Keeping in mind Puck's theory where IFFs exposure factors are linked with the matrix damage and the fiber/matrix de-bonding, whereas FFs are associated with the fiber damage.

### 3. Results and discussion

#### 3.1 Contact results in indentation

A preliminary study in the first step is conducted to determine the contact parameters. The objective of this step is to verify the accuracy of the model in the indentation step before undertaking the complete wear problem. For this purpose, normal force  $F_N$  was applied on the indenter as shown in Fig.5-a in section 2.1. Following contact parameters were evaluated:

- Total approach (depth of indentation) :  $\delta$
- Representative sizes of the contact area (major and minor axes): Parallel to the sliding direction denoted by  $2a$  and transverse to the sliding direction denoted by  $2b$
- Contact pressure profile and its maximum value:  $P_{\max}$

The contact parameters obtained from the FEM simulation of the indentation step are given in Table 3. In the figures for stress fields and damage exposure factors in section 3.2 and section 3.3, elliptical contact area has been shown with white color outline to elaborate the positions of the maximum values. These parameters are in agreement with the results found in the literature [9]. Hence, the FEM model is validated. For the AP-configuration, the penetration and the maximum contact pressure are slightly higher than the P-configuration. However, the difference

between the two configurations recorded is less than 10%. In both configurations, the contact surface is shorter in the stiffer fiber direction.

Keeping in view the material's characteristics (fiber diameter, fiber volume fraction) and the size of the contact area, the period of the material's microstructure  $L$  and that of the applied force  $L_w$  can be evaluated as  $8\ \mu\text{m}$  and  $120\ \mu\text{m}$ , respectively. Then the ratio  $L_w/L$  which characterizes the scale separation is 15 ensuring the efficiency of the homogenization scheme.

**Table 3:** Contact parameters during the indentation phase

Case	$\delta$ ( $\mu\text{m}$ )	$2a$ ( $\mu\text{m}$ )	$2b$ ( $\mu\text{m}$ )	$P_{\text{max}}$ (MPa)
P-configuration	2.249	60	70	638
AP-configuration	2.274	70	60	685

### 3.2 Stress results

The Von Mises equivalent stress counter has been plotted for the two configurations in both steps of indentation and sliding as given in Fig.6. It can be comprehended that these stress fields of the two configurations are identical at  $90^\circ$  rotation in the indentation step. However, due to the difference in the contact pressure during the indentation phase (Table 3), a small difference of the maximum values in stress is observed between the P and AP directions. In contrast, the Von Mises stress distributions are very different in the sliding steps for the two considered directions. Referring to Fig.6, the maximum Von Mises stress is located in the frontal part of the contact area for the P-configuration, whereas in case of the AP-configuration, it is located at the rear side of the contact area.

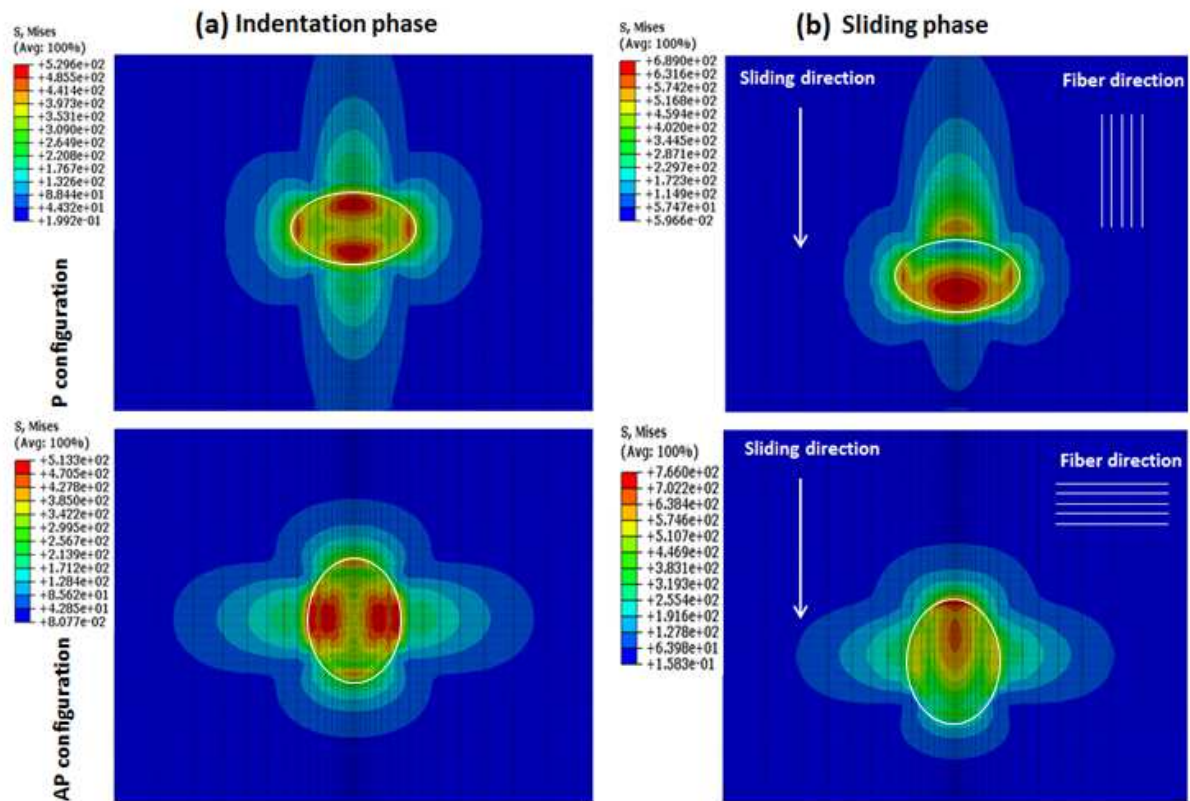


**Fig. 6:** Von Mises equivalent stress distribution for P and AP configurations, (a) indentation step, (b) sliding step

It is necessary to analyze the stress components in the local material coordinate system 1-2-3 (1: fiber direction, 2: transverse direction, 3: normal direction to the contact surface) in order to get a better interpretation in regards to the damage mechanisms based on the failure theories. For reasons of image quality, the FEM mesh is not shown. Instead, a view cut is used to visualize the contact stresses in the depth of the sample (see Fig.7 and Fig.8). The dotted line indicates the momentary position of the sliding counterpart with respect to the composite sample.

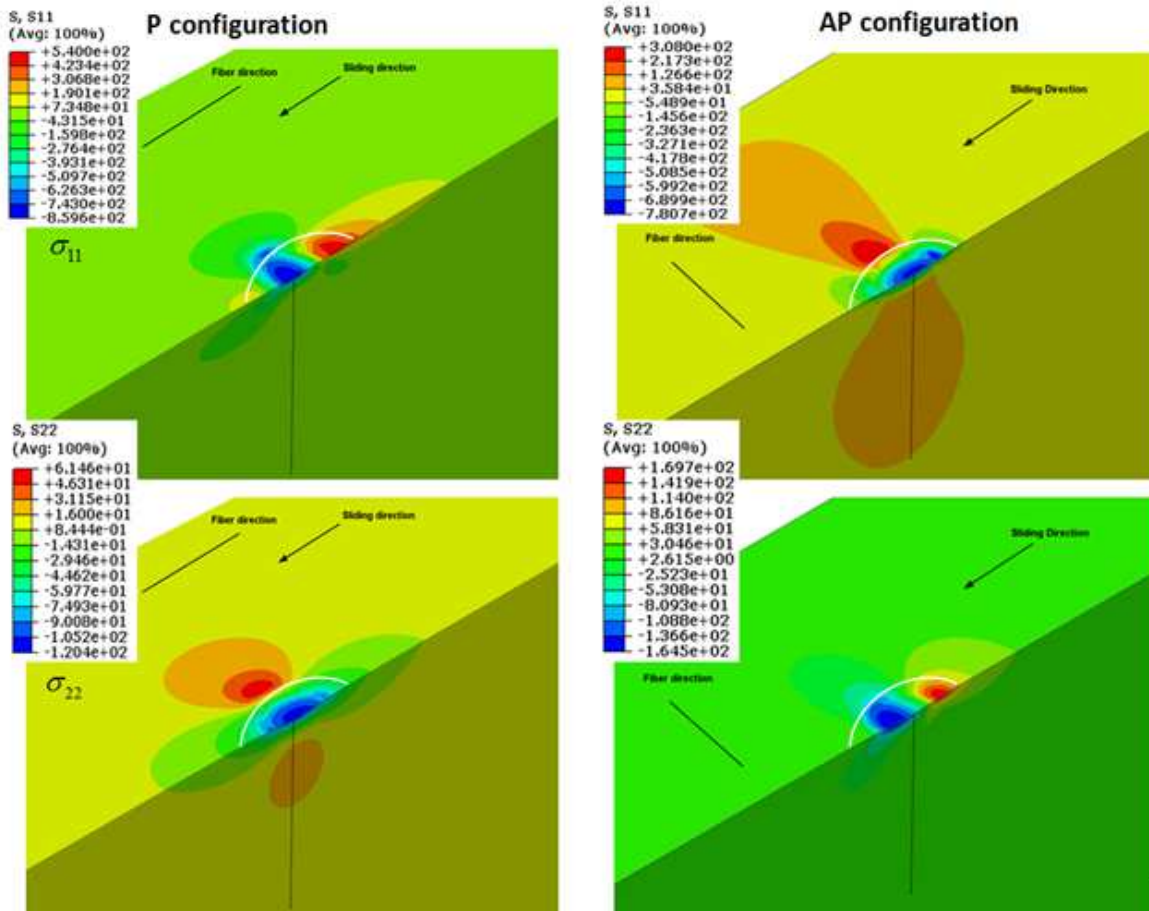


Fig. 7: Fiber direction and transverse direction stress distribution for the P and AP configurations in the sliding steps

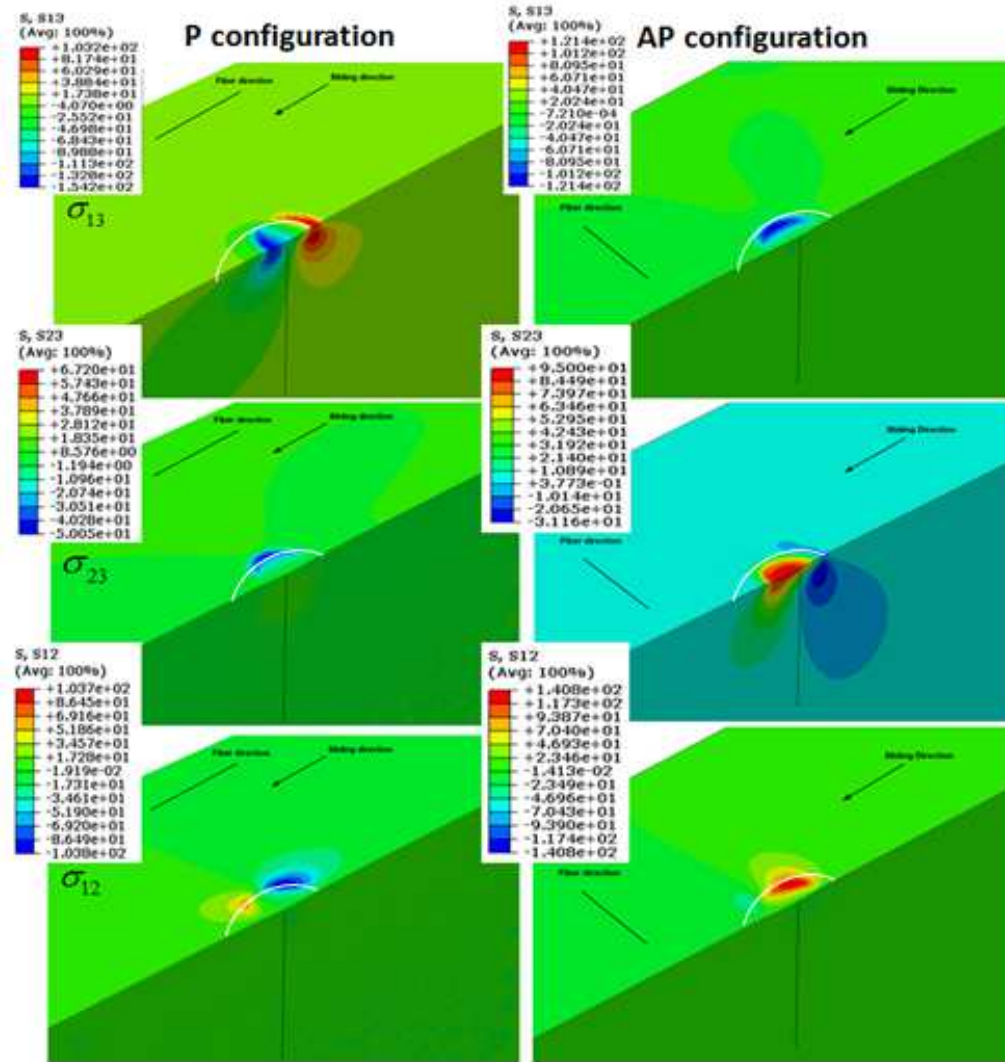


Fig. 8: Shear stress contours in the P and AP directions sliding

### 3.2.1 Parallel configuration

As seen in Fig.7 and the stress contours of  $\sigma_{11}$  and  $\sigma_{22}$  there in for the P-configuration, it can be noticed that the fibers are subjected to bending. This bending is produced by the contact pressure and its corresponding stresses under the contact zone including  $\sigma_{11}$ ,  $\sigma_{22}$ . Here  $\sigma_{11}$  is the axial compressive stress and  $\sigma_{22}$  is the transversal compressive stress. Along the depth of the composite specimen, transversal compression  $\sigma_{22}$  decreases and eventually transforms into traction. Similar stress patterns of  $\sigma_{11}$  and  $\sigma_{22}$  were observed in [9]. Higher tensile fiber stress  $\sigma_{11}$  and transverse stress  $\sigma_{22}$  are located in the vicinity of the contact zone. Due to the friction force, tension appears behind the contact area. In regards to shear stresses, the most dominant shear

stresses are  $\sigma_{12}$  and  $\sigma_{13}$  having values of 103 MPa, approximately. For  $\sigma_{12}$  shear stress, the maximum value is located on the surface at 45° direction behind the contact zone. The maximum of  $\sigma_{13}$  shear stress is also behind the contact zone but located below the contact surface.

### 3.2.2 Anti-parallel (AP) configuration

Under the contact zone (see Fig.7) for the AP-configuration, the fibers are under compression in a thin subsurface which was found as less than 10  $\mu\text{m}$ . Afterwards, the axial and transverse stresses,  $\sigma_{11}$  and  $\sigma_{22}$  respectively, change signs beyond this subsurface and become traction. The shear stress  $\sigma_{23}$  due to the friction is higher than the P-configuration having maximum value of 95 MPa as compared to the maximum value of 67 MPa for the sliding in the P-configuration. Similar to the P-configuration, the most dominant shear stresses are  $\sigma_{12}$  and  $\sigma_{13}$  having maximum value of 140 MPa. These are located in the vicinity of the contact zone.

Keeping in view the above stress analysis in the local material coordinate system, it is concluded that the stress magnitudes are higher in the AP-configuration than the P-configuration. This stress analysis is not sufficient to predict the nature of the damage that takes place when the rigid indenter is in contact with the composite specimen. Moreover, it is not very abstract to compare various stress components of the P-configuration with the AP-configuration unless a failure criterion is used which provides single scalar values by combining the stress components in a function. This function is known as stress exposure factor or damage exposure factor. For this purpose, an accurate failure theory is used to well understand the failure mechanisms that are induced during the contact of UD composite with the indenter. Hence, the damage exposure factors are determined based on the Puck's criterion in the sequel. The 3D Puck's theory is implemented with UMAT in ABAQUS.

### 3.3 Damage exposure factors

The four damage exposure factors of the Puck's theory (referred in Eqn.1) have been evaluated for the parallel (P) and anti-parallel (AP) configurations. When any of the stress exposure factors turns into unity, so it implies that the particular damage is going to take place in the undamaged material. To highlight the influence of the sliding, the exposure factors of FFs and IFFs during the indentation step and the sliding step are given separately for the P-configuration in Fig.9 and

Fig.10. In case of the AP-configuration these exposure factors are presented in Fig.12 and Fig.13.

In the indentation step, the same damage exposure patterns are found within a rotation of 90°. The difference in the values is due to the fact that the friction coefficient ( $\mu$ ) used for each configuration is not the same:  $\mu=0.28$  for the P-configuration and  $\mu=0.3$  for the AP-configuration. During the indentation step in both configurations, compressive damage of the fibers denoted by  $f_{E,FF,-}$  and compressive/shear damage of the matrix expressed by  $f_{E,IFF,-}$  appear in the contact zone. This is concluded on the basis that the stress exposure factors exceeded one which implies that these types of damages have occurred. Furthermore, tensile/shear matrix damage denoted by  $f_{E,IFF,+}$  has also been induced by the indentation. However, this damage is located outside the contact area (see Fig.10 and Fig.12). Keeping in view the values of the damage exposure factors reached during the indentation step, fiber failure due to the compressive stress is detected under the contact zone in addition to the fiber/matrix de-cohesion which appears along the fibers in the local vicinity of the contact zone (see,  $f_{E,IFF,+}$  distribution). Besides, compressive/shear matrix damage is observed under and around the contact area where the maximum values are at the border (see,  $f_{E,IFF,-}$  distribution).

### 3.3.1 Parallel configuration

In this section the damage exposure factors for the parallel configuration in sliding mode are compared with the indentation mode to highlight the influence of the frictional force that arises during sliding. Based on the results in Fig. 9-10, the frictional forces increased the damage exposure factors in a non-uniform fashion. During the sliding step, the tensile fiber damage exposure factor ( $f_{E,FF,+}$ ) increased by a factor of 3 and also the distribution changed as compared to the indentation step. The maximum value of  $f_{E,FF,+}$  in sliding is higher than the indentation:  $f_{E,FF,+}=0.34$  in indentation step and  $f_{E,FF,+}=1.04$  in sliding step. This is located behind the contact area. Hence, it indicates that fibers failed in tension at the rear side of the contact area. Considering the fiber failure under compression ( $f_{E,FF,-}$ ), the exposure factor increased with 37.6% and the failure appeared at the frontal contact zone. In regards to the matrix failure and fiber/matrix de-bonding, a similar pattern is obtained for the indentation and sliding steps. The damage exposure factors  $f_{E,FF,+}$  and  $f_{E,FF,-}$  increased by a factor of 1.7 and 1.2, respectively. The

maximum values are still located at the border of the contact zone. Among all the damage exposure factors, a less increase of about 17% in  $f_{E,FF,-}$  is noted.

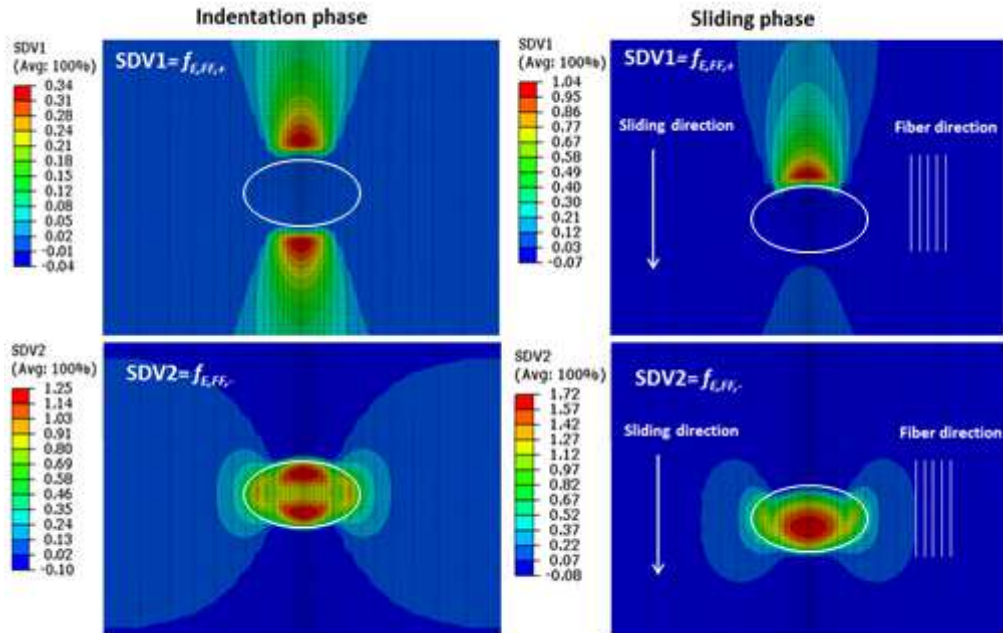


Fig. 9: Puck's FFs damage exposure factors (P-configuration)

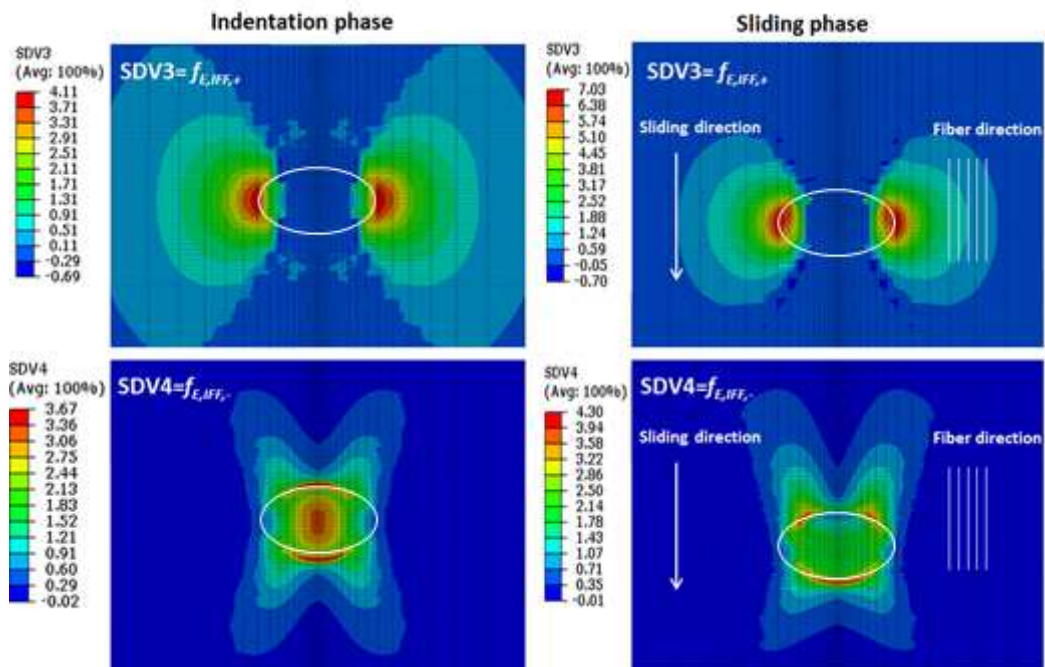
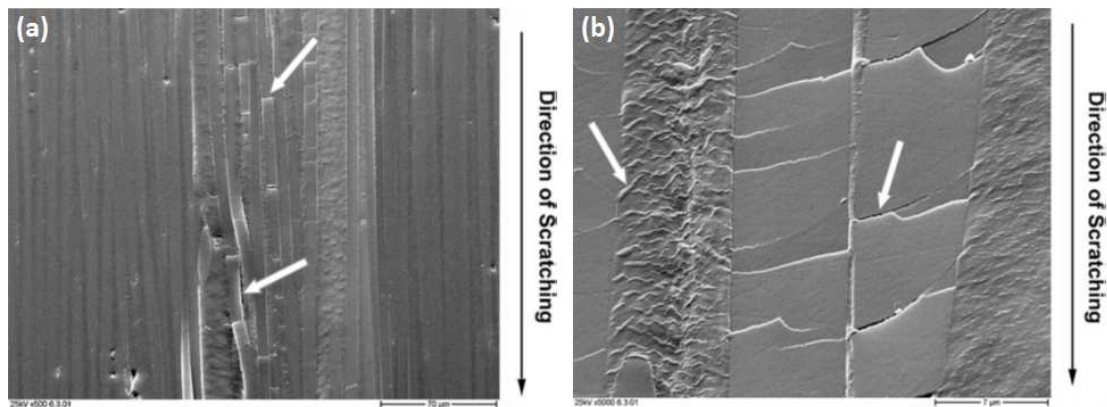


Fig. 10: Puck's IFFs damage exposure factors (P-configuration)

A scratch test in the fiber direction produced clear features of fiber/matrix de-bonding as illustrated in Fig.11. Due to the high tensile stresses, the edge of the contact area is visible by the de-bonding lines and fiber fractures can also be seen. In both figures, the formations of shear features of the matrix between the fibers are noticeable. These findings are in good agreement with the FE results discussed.



**Fig. 11:** (a) A single wear groove on a polished P direction CF/PEEK-surface (b) Failure mechanisms in the groove [9]

### 3.3.2 Anti-parallel (AP) configuration

In case of AP set-up, the same fiber exposure factors distributions are observed for the indentation and sliding steps. No tensile failure of the fibers is obtained because the value of  $f_{E,FF,+}$  is lower than 1. As for the indentation step, compressive fiber failure occurs with a minor increase in the value of the damage exposure factor of about 30%. However,  $f_{E,FF,-}$  obtained a uniform distribution in the central portion of the contact area. The sliding force increased the fiber-matrix de-cohesion exposure index  $f_{E,IFF,+}$  by a factor of 6, approximately. Referring to  $f_{E,IFF,-}$ , sliding leads to an increase of 69% in this particular damage exposure factor. Its distribution is very similar to the parallel configuration. It is evident that  $f_{E,IFF,-}$  can be regarded as a good indicator of the damage in matrix due to the sliding contact where both shear and transverse compression play their role in the damage development. Experimental observations also justify that when AP orientation scratch test is considered, the shear and the tension/compression type de-bonding are the most dominant wear mechanisms [9].

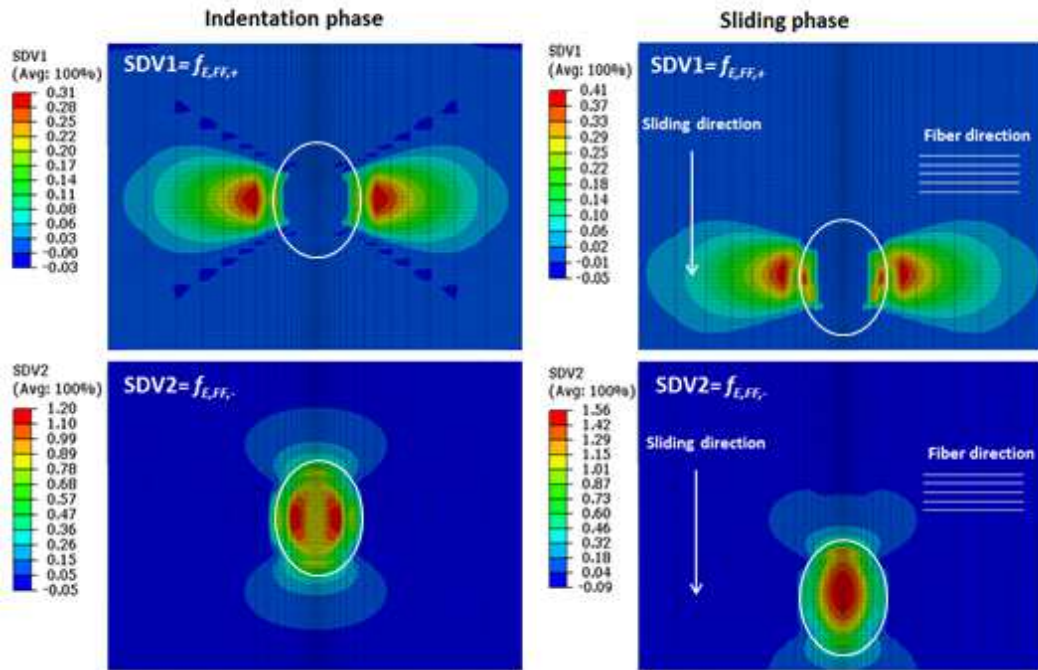


Fig. 12: Puck's FFs damage exposure factors (AP-configuration)

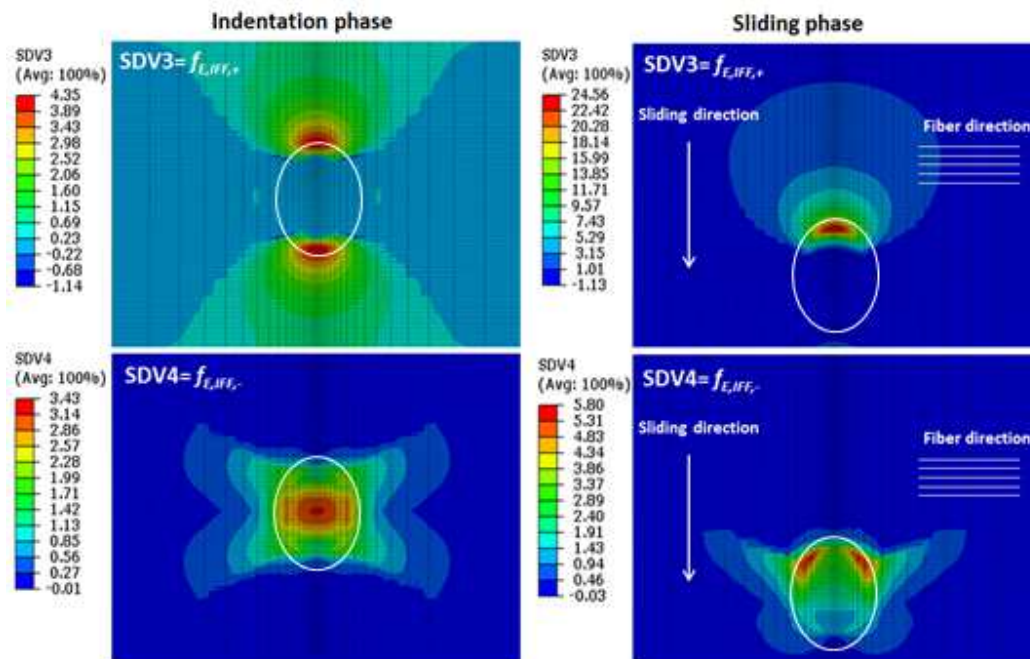


Fig. 13: Puck's IFFs damage exposure factors (AP-configuration)

The 3D topography of the damage zone after sliding is given for each configuration in Fig. 14. It was evaluated after removal of the elements in which  $f_{E,IFF,-}$  factor is higher than 1.

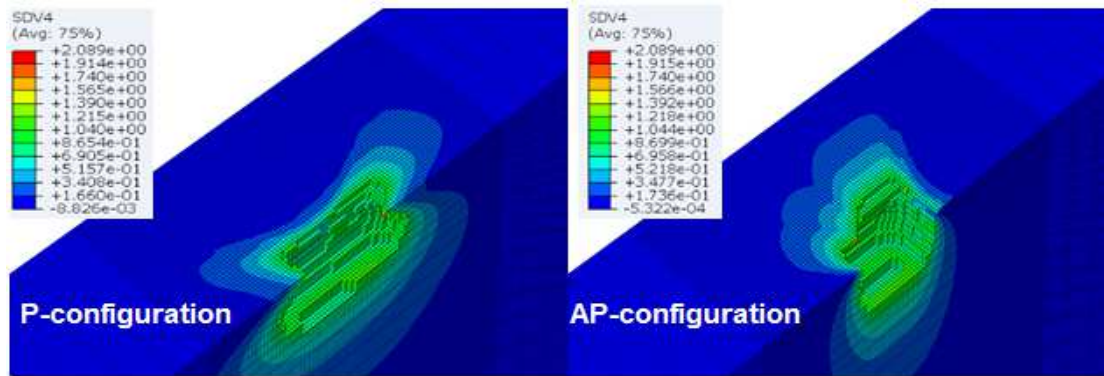


Figure 14: 3D topography of the damaged zone

The damage zone is longer in the P-configuration (0.17 mm) than the AP-configuration (0.13 mm). Whereas, it is wider for the AP-configuration (0.16 mm) as compared to the P-configuration (0.1 mm). The depth of the damage zone is approximately similar for both the configurations (0.063 mm).

Parametric sensitivity simulations have been carried out to highlight the effects of the friction coefficient  $\mu$  and normal load  $F_N$ . Considering the AP-configuration where the friction coefficient  $\mu$  is equal to 0.28 and the normal load  $F_N$  is equal to 1 N as the reference case, twelve simulations have been performed by varying  $\mu$  and  $F_N$  in the range of 0.15 to 0.35, and 0.25 to 2 N, respectively. The evolution of the damage exposure factors compared to the reference case has been illustrated in [Fig.15](#) and [Fig.16](#). It is clear that the friction coefficient has no effect on the fiber damage i.e. ( $f_{E,FF}$ ). However,  $F_N$  showed a considerable effect on both the damages of the fiber ( $f_{E,FF}$ ) and the matrix ( $f_{E,IFF}$ ).

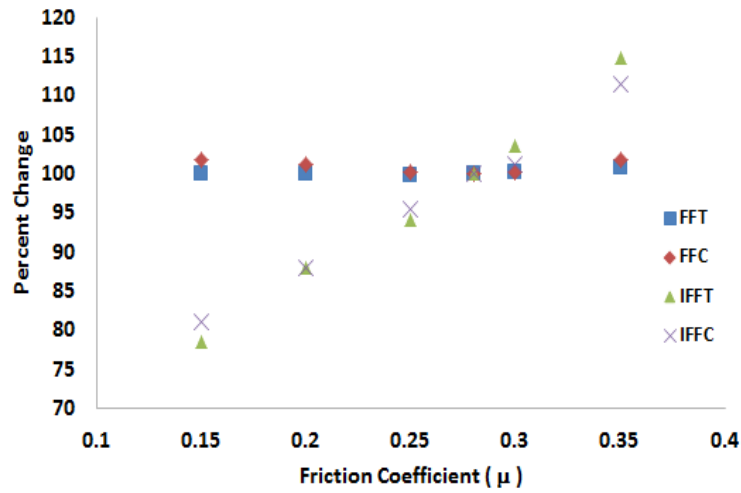


Figure 15: Effects of variation in friction coefficient on the damage exposure factors

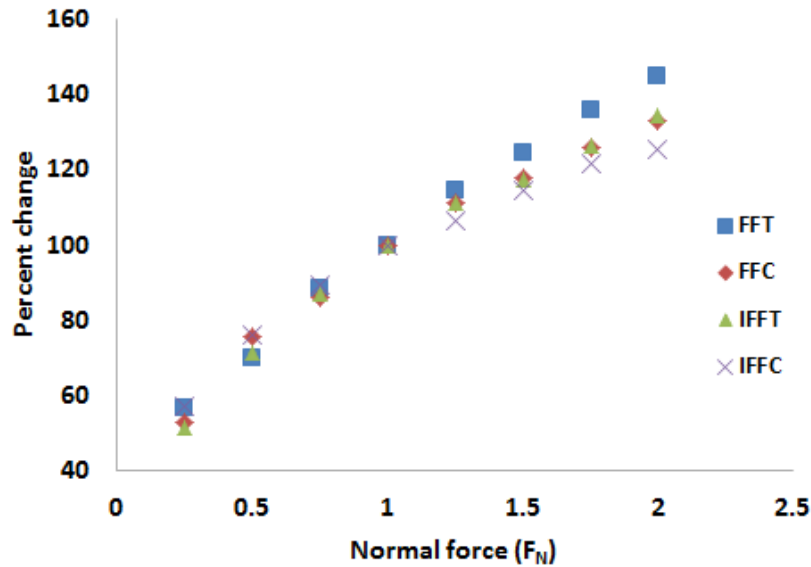


Figure 16: Effects of variation in normal force on the damage exposure factors

If we consider various fiber orientation angles ( $0^\circ$ ,  $15^\circ$ ,  $30^\circ$ ,  $45^\circ$ ,  $60^\circ$ ,  $75^\circ$ ,  $90^\circ$ ) with respect to the sliding direction, damage exposure factors can be evaluated with the present model during the sliding step. The values of the Puck's theory exposure factors determined based on the FEM are listed in Table 4. A significant increase in the damage exposure factors representing matrix cracks and fiber/matrix de-bonding in a collaborative way in tension denoted by  $f_{E,IFF,+}$  is clearly observed as the angle increases. This can be justified by the fact that the considered material has low fiber-matrix interface strength ( $R_{\perp}^I = 7$  MPa). A non-monotonic evolution is observed in the matrix damage caused by the compression and shear stresses ( $f_{E,IFF,-}$ ): an initial increase followed

by a decrease in which the maximum value is obtained at an angle of 60°. On the other hand, an inverse tendency is observed for tensile fiber damage exposure factor ( $f_{E,FF,+}$ ). A slight decrease is also obtained for the compressive fiber damage exposure factor ( $f_{E,FF,-}$ ).

**Table 4:** Failure exposure factor with respect to the fiber angle

<b>Fiber orientation</b>	$f_{E,FF,+}$	$f_{E,FF,-}$	$f_{E,IFF,+}$	$f_{E,IFF,-}$
<b>0°</b>	1.021	1.732	7.033	4.279
<b>15°</b>	1.010	1.719	9.779	4.79
<b>30°</b>	0.945	1.684	12.98	5.099
<b>45°</b>	0.832	1.640	17.21	6.011
<b>60°</b>	0.681	1.597	21.73	6.396
<b>75°</b>	0.535	1.572	24	6.188
<b>90°</b>	0.406	1.567	24.32	5.677

Puck's criterion seems appropriate to predict the contact damage which occurs during a scratch test. Based on these observations, it is possible to find a relationship between the damage exposure factors and wear. To study the wear and tribo-performance tests, different experimental set-ups are used. Pin-on-disc is one of the commonly followed tests for this purpose. It consists of a plane square stationary pin made of the sample material which is fixed and a normal force is applied on it. A disc is rotating and is in continuous frictional contact with the pin made of the materials of interest. The coefficient of friction ( $\mu$ ) is determined from the division of the tangential force measured by the known normal applied force. Sharma et al. [2] conducted experiments using pin-on-disc method for different off-axis angles of the fibers. The damage exposure factors are computed with this FEM model for the experiments of Sharma et al. [2] in the upcoming section.

### 3.4 Damage exposure factors vs Specific wear rate

In the experiment of pin-on-disc, pin is made of the composites of interest which is slid against a smooth disc of mild steel. After experiment, pin is cleaned, dried and weighed to measure the loss in material during the wear process. The specific wear rate denoted by  $K_0$  is calculated using the following equation:

$$K_0 = \frac{\Delta m}{\rho F d} \quad (m^3 / N.m) \quad (5)$$

Where  $\Delta m$  is the weight loss in kg,  $\rho$  is the density in kg/m<sup>3</sup>,  $F$  is the applied normal load in Newton (N) and  $d$  is the sliding distance in meters (m). Generally, this is performed for different load and velocity. Sharma et al. [2] studied the tribological performances of CF-PEI as a function of the fiber orientation angles (0°, 15°, 30°, 45°, 60°, 75° and 90°) with respect to the sliding directions. The pin size was 10 x 10 x 5 mm<sup>3</sup> and three normal loads were applied, viz. 200 N, 300 N and 400 N. For each test, the friction coefficient ( $\mu$ ) was recorded and is used here in the FEM simulation. In the experiments, they observed that specific wear rate increased with the fiber orientation as rendered in Fig. 17. The authors reported that fibers in transverse direction proved poorest in tribological characteristics. Conversely, they observed very low wear rate for composite with sliding parallel to fibers. It is important to highlight that the main characteristic of this material is that in severe loading conditions (normal load of 400 N), wear decreased further confirming the suitability of this composite as a dry bearing material for severe operating conditions (see Fig. 17).

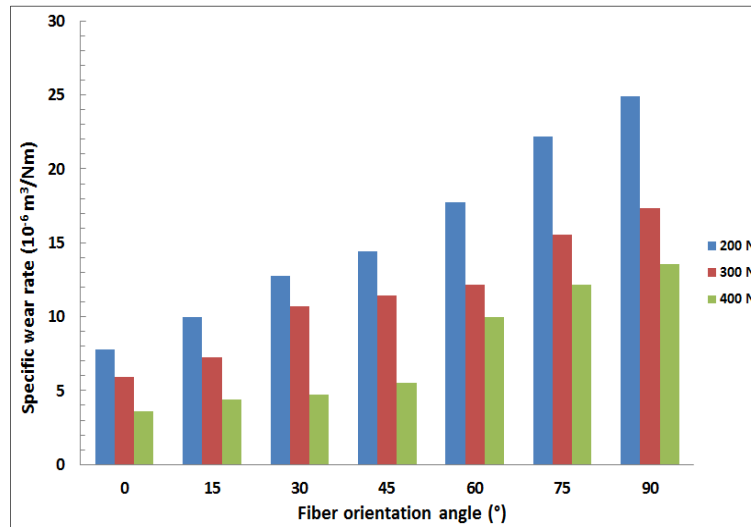


**Fig. 17:** Specific wear rate as a function of the fiber orientation angle [2]

A pressure corresponding to the normal force divided by the surface of the sample and a tangential pressure corresponding to the pressure multiplied by the friction coefficient were applied uniformly to the contact surface. The assumption of uniform pressure is viable because prior to the experiment, the pin was slid against a rough mild steel disc of  $R_a$  value 0.3–0.4  $\mu\text{m}$  to obtain a uniform contact. To compare the specific wear rate with the damage exposure factors qualitatively, we defined the specific Puck damage exposure factor as the ratio between the damage exposure factor and the applied normal load. In the case of a plane square pin, the highest exposure factor was obtained for the matrix damage under compression and shear mode expressed as  $f_{E,IFF,-}$ . In Fig. 18, the specific Puck damage indicator associated with  $f_{E,IFF,-}$  as a function of the normal load and the fiber orientation angle is shown. It is evident that the same tendency as compared to the specific wear rate in the experiments was obtained.

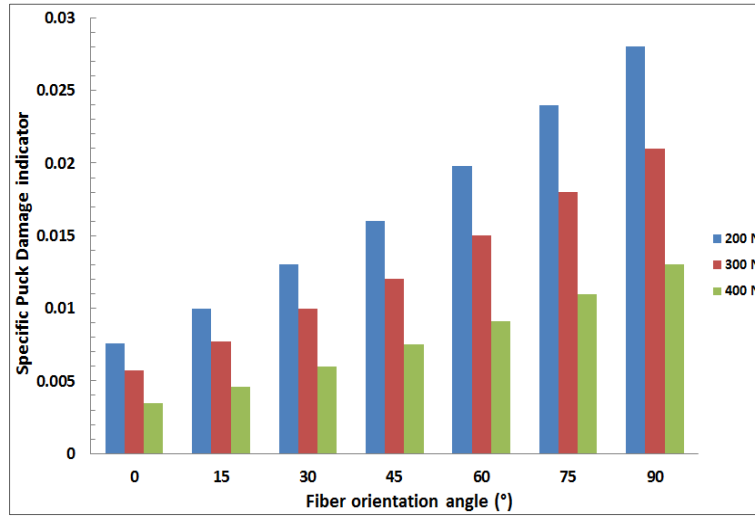


**Fig. 18:** Specific Puck damage indicator ( $f_{E,IFF.}/F$ ) as a function of the fiber orientation angle

The specific damage factors obtained for the AP-configuration (fiber orientation angle of  $90^\circ$ ) are very high compared to the P-configuration (fiber orientation angle of  $0^\circ$ ). This can be explained by the analysis of the stresses in each configuration. Fig. 19 is a simplified representation of the stresses that are acting in each sliding configuration.  $\sigma_{22}$  is the normal stress due the contact pressure and  $\sigma_{12}$ ,  $\sigma_{23}$  are the shear stresses due to the frictional force in cases of the parallel and the anti-parallel sliding modes, respectively. The normal of the contact surface bounded by the vertices A, B, C and D is along the 2-axis in Fig. 19 on which the stresses are acting: (a) Parallel configuration stress state ( $\sigma_{22}$ ,  $\sigma_{12}$ ), (b) anti-parallel configuration stress state ( $\sigma_{22}$ ,  $\sigma_{23}$ ).

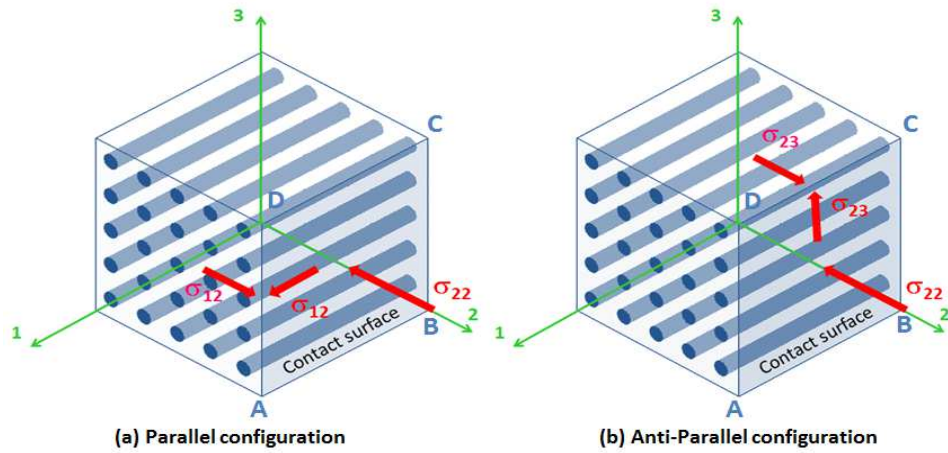


**Fig. 19:** Simplified representation of the stresses on the contact surface bounded by the vertices A, B, C and D in the two sliding configurations

In case of parallel configuration for the same applied contact pressure ( $\sigma_{22} < 0$ ), it is apparent that the shear stress  $\sigma_{12}$  is in-plane. Whereas, it is out-of-plane shear  $\sigma_{23}$  when sliding in the anti-parallel configuration is considered. It is well-known that FRPs composites are usually weaker in out-of-plane shear in comparison to the in-plane shear stress. Accordingly, referred to [Table 1](#), the out-of-plane shear strength is also lower for the chosen material than the in-plane shear strength. This results in higher damage exposure factors in the AP direction.

In [Fig. 17](#) and [Fig.18](#), specific wear rate and the specific Puck damage indicator ( $f_{E,IFF,-} / F$ ) decreased with applied load. In other words, the more severe the conditions of loading, the better are the tribo-performance of the composites. Hence, the more the normal applied load the more is the wear resistance. Using Hashin's criterion, Panier et al. [\[24\]](#) showed that this tendency cannot be explained by FEM modeling (see [Fig. 20](#)). Consequently, Puck's criterion is better to be used here which is able to predict the experimental trends of the increase in wear resistance by the increase in the normal compressive load.

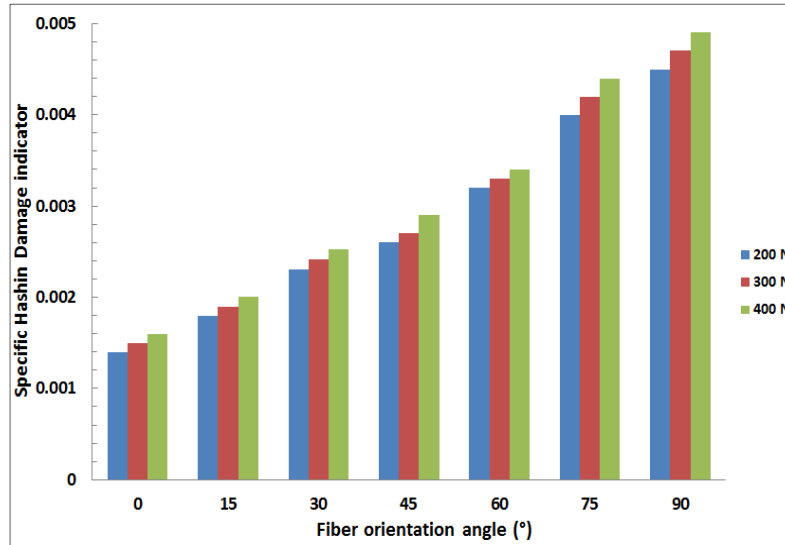


**Fig. 20:** Specific Hashin's compressive matrix damage indicator as a function of fiber orientation angle

In fact, Puck's criterion takes into account that the material shear strength increases with the increase in the compressive transverse stress  $\sigma_{22}$  (Fig.21). This implies that due to the enhanced friction in the material surfaces during higher transverse compression, the material is able to transfer more shear stress as compared to the lower transverse compression. Thus, higher the contact pressure, the higher the enhancement in the shear strength of the material. Still, there exists a critical limit of compressive  $\sigma_{22}$  beyond which no increase in the shear strength is possible [16, 18]. Subsequently, shear strength starts decreasing when compressive stress  $\sigma_{22}$  crosses the critical limit. This can be better visualized by comparing the failure envelopes of Puck's theory which is based on Mohr-Coulomb hypothesis with the Hashin's theory. In Fig.21, for a contact pressure between 0 and 58 MPa (i.e.  $-58 < \sigma_{22} < 0$  MPa) the shear strengths  $\sigma_{12}$  and  $\sigma_{23}$  increase to 38 MPa (point P) and 28 MPa (point Q), respectively. In contrary, no enhancement in the shear strength can be observed based on the Hashin's theory envelope in Fig.21.

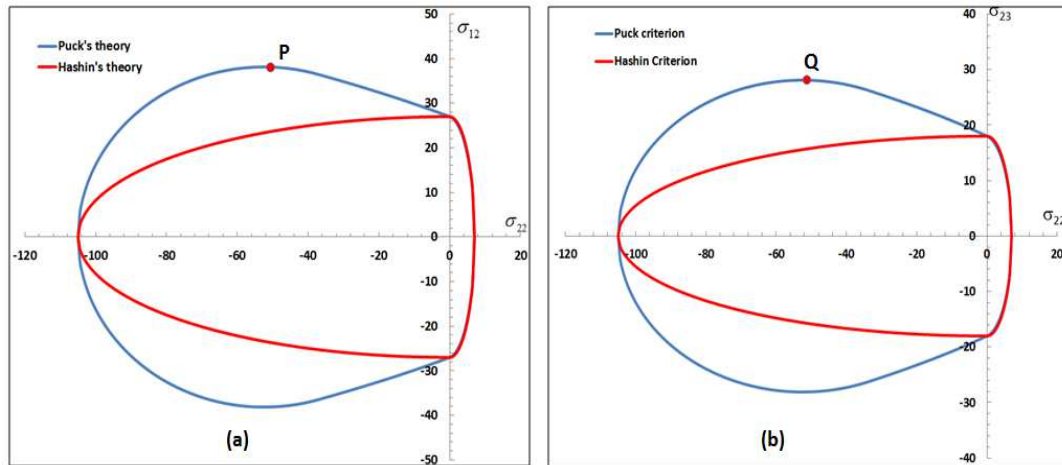


**Fig. 21:** Puck's and Hashin's criteria (a)  $\sigma_{22}$ ,  $\sigma_{12}$  stress space, (b)  $\sigma_{22}$ ,  $\sigma_{23}$  stress space

## 4. Conclusions

The phenomenon of adhesion wear in UD laminate and the types of damage mechanisms induced in the indentation and adhesion wear during sliding in CF-PEI against steel indenter were studied. 3D Puck's theory was employed which is best suited for the accurate prediction, particularly, in case of transverse compression which prevails in the contact and wear phenomenon. Thanks to the capability of Puck's theory to capture the enhancement in shear strength with the increase in the transverse compressive stress, the FEM results were in excellent agreement with the experimental results in a qualitative manner. The trends showed better correspondence as the orientation of the angle between the fiber and the direction of sliding was varied. In regards to the tribological performance, the orthogonal sliding with respect to fiber resulted into higher damage exposure factors and hence higher subsequent wear rate. In case of parallel sliding, the normal and frictional forces were transferred by the stiffer fibers. Therefore, FRPs were less exposed to the damage mechanisms in the parallel configuration sliding.

### Acknowledgments

The corresponding author (**ISRAR UD DIN**) is thankful to the **Higher Education Commission (HEC), Pakistan**, and **Campus France** for the provision of financial support to his doctoral studies based in **France**.

### References

- [1] Bijwe JR, Rekha. Carbon fabric reinforced polyetherimide composites: Optimization of fabric content for best combination of strength and adhesive wear performance. *Wear*. 2007;262:749-58.

- [2] Sharma M, Rao IM, Bijwe J. Influence of orientation of long fibers in carbon fiber–polyetherimide composites on mechanical and tribological properties. *Wear*. 2009;267:839-45.
- [3] Wieleba W. The Mechanism of Tribological Wear of Thermoplastic Materials. *Archives of Civil and Mechanical Engineering*. 2007;7:185-99.
- [4] Lu Z, Friedrich K, Pannhosrt W, Heinz J. Wear and Friction of unidirectional carbon fiber-glass matrix composite against various counterparts. *Wear*. 1993;162:1103-13.
- [5] Cirino M, Friedrich K, Pipers R. The effect of fiber orientation on the abrasive wear behavior of polymer composite materials. *Wear*. 1988;121:127-41.
- [6] Rodríguez-Temblequ LA, MH. Friction and Wear Modelling in Fiber-Reinforced Composites. *CMES*. 2014;102:183-210.
- [7] Friedrich K, Fakirov S, Zhang Z. *Polymer Composites: From Nano- to Macro-scale*: Springer, 2005.
- [8] Sharma M, Mohan Rao I, Bijwe J. Influence of fiber orientation on abrasive wear of unidirectionally reinforced carbon fiber–polyetherimide composites. *Tribology International*. 2010;43:959-64.
- [9] Friedrich K, Varadi K, Goda T, Giertsch H. Finite element analysis of a polymer composite subjected to a sliding steel asperity. *Materials Science*. 2002;37:3497-507.
- [10] Ovaert T. Wear of Unidirectional Polymer Matrix Composites with Fiber Orientation in the Plane of Contact. *Tribology Transactions*. 1997;40:227-34.
- [11] Mzali S, Elwasli F, Mkaddem A, Mezlini S. A micromechanical scratch model to investigate wear mechanisms in UD-GFRP composites. *Mechanics & Industry*. 2018;19:305.
- [12] Johnson GC, WH. A constitutive model and data for metals subjected to large strains, high strain rates and high temperatures. 7th International Symposium on Ballistics. Netherlands 1983. p. 541-7.
- [13] Ud Din I, Hao P, Franz G, Panier S. Elastoplastic CDM model based on Puck’s theory for the prediction of mechanical behavior of Fiber Reinforced Polymer (FRP) composites. *Composite Structures*. 2018;201:291-302.
- [14] Lee C-S, Kim J-H, Kim S-k, Ryu D-M, Lee J-M. Initial and progressive failure analyses for composite laminates using Puck failure criterion and damage-coupled finite element method. *Composite Structures*. 2015;121:406-19.
- [15] Reinoso J, Catalanotti G, Blázquez A, Areias P, Camanho PP, París F. A consistent anisotropic damage model for laminated fiber-reinforced composites using the 3D-version of the Puck failure criterion. *International Journal of Solids and Structures*. 2017;126-127:37-53.
- [16] Puck AS, H. . Failure analysis of FRP laminates by means of physically based phenomenological models. *Composite Science and Technology*. 2002;62:1633-62.
- [17] Hashin Z. Failure criteria for unidirectional fiber composites. *Applied Mech-Trans ASME*. 1980;47 (2):329-34.
- [18] Puck A, Kopp J, Knops M. Guidelines for the determination of the parameters in Puck’s action plane strength criterion. *Composite Science and Technology*. 2002;62:371-8.
- [19] Hinton MJ KA, Soden PD. Failure criteria in fibre reinforced polymer composites: The World Wide Failure Exercise UK: Elsevier 2004.
- [20] Soden PD, Hinton MJ, Kaddour AS. Lamina properties, Lay-up configurations and loading conditions for a range of fiber-reinforced composite laminates. *Composite Science and Technology*. 1998;58:1011-22.
- [21] Soden PD, Hinton MJ, Kaddour AS. A comparison of the predictive capabilities of current failure theories for composite laminates. *Composite Science and Technology*. 1998;58:1225-54.
- [22] Hinton MJK, A. S. The background to Part B of the Second World-Wide Failure Exercise: Evaluation of theories for predicting failure in polymer composite laminates under three-dimensional states of stress. *Journal of Composite Materials*. 2013;47:643-52.
- [23] Matthias Deuschle HK, Bernd- H. Finite element implementation of Puck’s failure theory for fibre-reinforced composites under three-dimensional stress. *Journal of Composite Materials*. 2012;46:2485-513.
- [24] Panier S, Franz G, Bijwe J, Hui L. Finite Element Analysis of the damage occurring in the sliding contact between a metallic ball and a composite plate. *Proceedings of Asia International Conference on Tribology*. Malaysia.2018. p. 246-7.